

Quantum annealing with ultracold atoms in a multimode optical resonator

Valentin Torggler, Sebastian Krämer, and Helmut Ritsch
Institut für Theoretische Physik, Universität Innsbruck, A-6020 Innsbruck, Austria

A dilutely filled N -site optical lattice near zero temperature within a high- Q multimode cavity can be mapped to a spin ensemble with tailorable interactions at all length scales. The effective full site to site interaction matrix can be dynamically controlled by the application of up to $N(N+1)/2$ laser beams of suitable geometry, frequency and power, which allows for the implementation of quantum annealing dynamics relying on the all-to-all effective spin coupling controllable in real time. Via an adiabatic sweep starting from a superfluid initial state one can find the lowest energy stationary state of this system. As the cavity modes are lossy, errors can be amended and the ground state can still be reached even from a finite temperature state via ground state cavity cooling. The physical properties of the final atomic state can be directly and almost non-destructively read off from the cavity output fields. As example we simulate a quantum Hopfield associative memory scheme.

The realization of strong collective coupling between ultra-cold atoms and the electromagnetic field in a Fabry-Pérot cavity [1] opens a unique test ground to study the real time dynamics of quantum phase transitions in open systems of mesoscopic size [2–9]. Cavity field mediated interactions induce a variety of self-ordered phases where the particles break the translational symmetry by forming complex spatial patterns [1, 10–13]. In a first seminal experiment at ETH the first controllable quantum simulation of the superradiant Dicke phase transition was demonstrated as predicted for the Tavis-Cummings model several decades ago [6, 14]. By adding an extra optical lattice in the cavity, the complex phase diagram of a Bose-Hubbard Hamiltonian with tailorable short and infinite range interactions was then experimentally studied in great detail, exhibiting superfluid, insulator and supersolid regions [15]. The experiment shows very good agreement with theoretical models using various approximate numerical methods like dynamical mean field approaches, predicting a supersolid phase region [16, 17].

In recent work we exhibited that versatility and complexity of the lattice cavity system strongly increase by adding extra pump laser frequencies close to resonance with different cavity modes [18]. For classical point particles one finds that the coupled atom cavity dynamics can be designed as a selfoptimizing light collection system with learning and memory capacity [19]. Similarly, generalizing the system to fixed multilevel atoms and using degenerate modes, Gopalakrishnan and coworkers previously proposed to simulate a quantum version of the Hopfield model [20–22]. Applications to study the physics of a Bose glass were also suggested [23].

As the scattered light contains information on the atoms' quantum statistical properties, one can perform minimally perturbing observations in real time and use quantum measurement back action and feedback to further control the system [24, 25]. First experimental studies of multimode systems were also reported recently [26].

For a single laser frequency the interaction between the atoms induced by a single cavity mode is spatially periodic and infinite range [1]. In contrast we show that

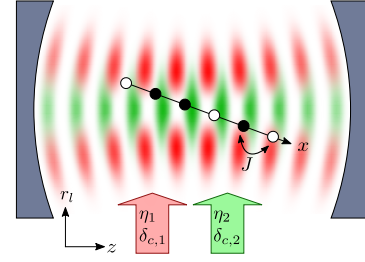


FIG. 1. A partially filled optical lattice with N sites inside a multimode optical resonator is pumped from the side by several lasers with frequencies close to cavity resonances.

by help of several pump laser frequencies and tailored illumination geometries, the coupling strengths and light shifts at different sites can be individually modified in such a form as to implement a full connectivity matrix between all lattice sites. In the limit of strong on-site repulsion and low density, one gets only zero or one atom per site mimicking a pseudo spin lattice. At least in principle any coupling matrix can be realized using order N^2 cavity modes [27]. Note that our approach does not need auxiliary qubits to realize long-range coupling, in contrast to current implementations [28], which use minor embedding [29], or alternative architectures [30].

As power and frequency of the pump lasers can be externally controlled in real time, we have a natural and straightforward way to implement quantum annealing [31, 32]. One simply slowly increases the strength of the pump lasers in the system to adiabatically reach the ground state of the coupled spin Hamiltonian. As we have a genuine open system, our implementation also suggests a new route towards quantum simulation in a driven-dissipative system as small errors during the sweep process can be amended via cavity ground state cooling [33] when we operate the lasers red detuned. This is the more effective the more laser modes we have available for coupling and cooling.

This work is organized as follows: after introducing the general multimode atom-field Hamiltonian and its trun-

cated Bose-Hubbard form, we map it to a coupled spin model in the strong on-site interaction limit. Spin-spin coupling arises from cavity enhanced light scattering and we exhibit how any desired coupling matrix can be found by proper mode choice. Finally as generic non trivial example we simulate a Hopfield associative memory model via quantum annealing [34].

Model.—We study a 1D optical lattice with N_A atoms trapped in $N > N_A$ sites, placed inside an optical resonator supporting many modes (see figure 1). The atoms are directly illuminated by several lasers with frequencies close to the resonance of corresponding cavity modes. For sufficient mode spacing, light from each laser is scattered into one specific mode only and scattering between different modes is suppressed. Furthermore, the laser frequencies are far away from any internal atomic resonance to allow for elimination of the inner atomic degrees of freedom.

The single particle Hamiltonian for an atom with mass m_A then reads [35]

$$H_0 = \frac{\hat{p}^2}{2m_A} + V_L \cos^2(k_L \hat{x}) - \hbar \sum_m \delta_{c,m} a_m^\dagger a_m + \hbar \sum_m \eta_m (u_{p,m}^*(\hat{x}) u_{c,m}(\hat{x}) a_m + \text{h.c.}), \quad (1)$$

where we neglect the atomic state dependent dispersive shifts of the cavity modes. The operators \hat{x} and \hat{p} are position and momentum operators along the lattice axis x , while a_m denotes the annihilation operator of the m -th mode. The normalized mode functions of pump and cavity modes are $u_{p,m}(x)$ and $u_{c,m}(x)$ and the real valued parameters η_m are effective pump strengths. $\delta_{c,m}$ is the laser-cavity detuning of the m -th mode and the optical lattice of depth V_L is created by an extra standing wave with wave number k_L .

For the many-particle Hamiltonian in second quantization formalism in the tight binding limit and neglecting cavity modifications of the tunneling we obtain the generalized intra-cavity Bose-Hubbard Hamiltonian [35–37]

$$H = H_{BH} - \hbar \sum_m \delta_{c,m} a_m^\dagger a_m + \hbar \sum_m \left(\eta_m \sum_i ((v_m^i)^* a_m + v_m^i a_m^\dagger) \hat{n}_i \right) \quad (2)$$

with the standard Bose-Hubbard Hamiltonian

$$H_{BH} = -J \sum_i (b_{i+1}^\dagger b_i + b_i^\dagger b_{i+1}) + \frac{U}{2} \sum_i \hat{n}_i (\hat{n}_i + 1). \quad (3)$$

Note that lattice and cavity directions can be chosen independently. The geometry of the modes (i.e. the mode functions and laser illumination directions) only enters via the N -dimensional coupling amplitude vectors \mathbf{v}_m , with their components given by

$$v_m^i = \int dx w^2(x - x_i) u_{p,m}(x) u_{c,m}^*(x), \quad (4)$$

where $w(x - x_i)$ is the Wannier function for an atom at a given site i . For consistency of the model we also assume that the optical lattice is deeper than the light shifts induced by the dynamical cavity field intensity, so that the Wannier function $w(x)$ depends on the prescribed lattice geometry only. J and U describe nearest neighbor tunneling rate and the on-site interaction strength [38].

For a given atomic distribution the balance between gain from coherent scattering and decay through the mirrors with rates $2\kappa_m$ leads to the steady state fields

$$a_m = \eta_m \sum_i v_m^i \hat{n}_i / (\delta_{c,m} + i\kappa_m). \quad (5)$$

Hence the cavity output fields directly represent the atomic density distribution in the lattice. In the bad cavity limit $\hbar\kappa_m \gg J, U$ the cavity fields follow the atomic distribution almost instantaneously, which allows for extracting the atomic dynamics in real time. Often the cavity modes can be adiabatically eliminated resulting in an atomic effective Hamiltonian

$$H_{ad} = H_{BH} - \zeta \sum_{i,j} A_{ij} \hat{n}_i \hat{n}_j. \quad (6)$$

The interesting part of the physics is encoded in the real and symmetric interaction matrix

$$A = \sum_m (f_m / \zeta) V_m \quad (7)$$

with an effective interaction strength $\zeta = \|\sum_m f_m V_m\|$. Thereby each single mode contributes to A with the single mode interaction matrix

$$V_m = \text{Re}(\mathbf{v}_m \otimes \mathbf{v}_m^*), \quad (8)$$

where \otimes denotes the outer product. The strength and sign are controlled by the input parameters $f_m = -\hbar\delta_{c,m}\eta_m^2/(\delta_{c,m}^2 + \kappa_m^2)$. Since these parameters depend on detuning and amplitude of the pump lasers, one can externally manipulate A without any change of the setup.

So far we have a quite general coupled quantum oscillator implementation in which the state of each oscillator is given by the occupation number at a lattice site. By increasing the on-site interaction $U \gg J, \zeta$ the oscillators get nonlinear and the extra energy required for multiple occupation of a site gets large. Consequently, for low enough densities only zero or single occupations occur and the bosonic creation and annihilation operators can be mapped to spin-1/2 operators, identifying an occupied site with spin-up and an empty site with spin-down. Using $b_i \rightarrow \sigma_i$ and $\hat{n}_i \rightarrow \frac{1}{2}(\sigma_i^z + 1)$, where σ_i^α are Pauli matrices and $\sigma_i = \frac{1}{2}(\sigma_i^x - i\sigma_i^y)$, transforms our Hamiltonian into a coupled spin model

$$H_{sp} = -J \sum_i (\sigma_{i+1}^\dagger \sigma_i + \sigma_i^\dagger \sigma_{i+1}) - \frac{\zeta}{4} \left(\sum_{i,j} A_{ij} \sigma_i^z \sigma_j^z + \sum_i \left[2 \sum_j A_{ij} \right] \sigma_i^z \right). \quad (9)$$

An equivalent model appears for polarized fermions in the lattice. Since H_{sp} commutes with $\sum_i \sigma_i^z$ the accessible Hilbert space reduces to the $\binom{N}{N_A}$ -dimensional subspace with fixed number of spin-up particles.

Constructing an interaction matrix.—Let us now investigate how to realize a general interaction matrix A . While its off-diagonal elements determine the interaction between two pseudo-spins, the diagonal elements specify the local field strengths in the second line of eq. (9). Specifically, a local field strength on the i -th spin $h_i := 2 \sum_j A_{ij}$ corresponds to the diagonal element $A_{ii} = h_i/2 - \sum_{j \neq i} A_{ij}$ in the matrix. Hence, in order to have full control over interactions and local fields we have to specify up to $N(N+1)/2$ elements, which in the worst case requires as many lasers. Luckily here these are classical fields with fixed amplitude and frequency.

Formally, the interaction matrix (7) appears as linear combination of matrices V_m with coefficients f_m/ζ . Thus if we manage to choose mode functions $u_{c,m}$, pump fields $u_{p,m}$ and lattice location such that $\{V_m\}_{m=1, \dots, N(N+1)/2}$ forms a basis of the real symmetric matrices, eq. (7) can be inverted to fix the required input parameters

$$f_m(A) = \zeta \sum_n (G^{-1})_{mn} \langle V_n, A \rangle. \quad (10)$$

Here G is the Gram matrix $G_{mn} = \langle V_m, V_n \rangle$ with inner product $\langle A, B \rangle = \text{Tr}(AB^\dagger)$. In other words, once a set of modes forming a basis is found, we can directly determine the input laser properties to realize an arbitrary interaction matrix A . While $N(N+1)/2$ lasers are needed to get a complete basis set, many interesting interaction matrices can be constructed with a lot less modes.

Annealing dynamics.—In principle our setup realizes an effective spin Hamiltonian with general time dependent all-to-all spin interactions and local fields, resembling an infinite-range Sherrington-Kirkpatrick model [39]. This allows for quantum simulation and encoding classical optimization problems in its ground state. The numerically non-trivial task of finding the ground state of a Hamiltonian H_p is tackled by quantum annealing [31, 32, 40], which might promise a speedup over classical methods [41–43]. To this end one adiabatically evolves the system with a time-dependent Hamiltonian

$$H_{QA}(t) = a(t)H_{kin} + b(t)H_p. \quad (11)$$

The kinetic term H_{kin} is chosen simple enough to possess a known gapped ground state. Initially at $t = 0$, the first term is dominant, i.e. $a(0) \gg b(0)$ and the system is prepared in this ground state of H_{kin} . By slowly decreasing $a(t)$ and increasing $b(t)$ the second term becomes dominant after an annealing time τ , i.e. $a(\tau) \ll b(\tau)$. Due to the adiabatic theorem [44] the system approximately stays in its instantaneous eigenstate and thus finally ends up in the ground state of H_p , provided τ is large enough, i.e. the adiabatic passage is slow.

Note that our Hamiltonian H_{sp} (9) with time-dependent coefficients $\zeta(t)$ and $J(t)$ already has the genuine form of a quantum annealing Hamiltonian H_{QA} , where the first line corresponds to H_{kin} and the second line to H_p . In adiabatic transfer we ramp up $\zeta(t)$ from $\zeta(0) = 0$ until the kinetic term becomes negligible, i.e. $\zeta(\tau) \gg J$. This can be achieved by uniformly increasing all $|f_m|$'s, i.e. physically by (i) increasing the strengths of all pump lasers or (ii) tuning them closer to resonance with the cavity modes. The uniformity guarantees that A and thus the structure of H_p is not changed during the sweep. A simultaneous increase of the lattice depth to reduce tunneling J helps further. In our open system the final state readout can be done by analyzing the light leaking out from the cavity and inverting the overdetermined linear system of eq. (5).

Note that instead of adiabatic transfer one could implement cavity cooling for the full interacting Hamiltonian to cool towards the ground state starting from a thermal state. This has proven successful for the single mode case [33, 45] and cooling profits from more modes [1].

Associative memory.—As a generic example we consider a Hopfield associative memory network with quantum annealing recall [34, 46]. A Hopfield net consists of N binary state units (so-called neurons), which can be represented by (classical) Ising spins s_i interconnected by real symmetric weights W_{ij} . For their dynamics Hopfield proposed an iterative update rule, which locally minimizes an energy function $E(\mathbf{s}) = -\sum_{i < j} W_{ij} s_i s_j$ of the system state vector \mathbf{s} . In combination with a learning rule for determining the weights W_{ij} the network works as an associative memory, which can memorize a set of P states $\mathcal{M} = \{\mathbf{w}_p\}_{p=1, \dots, P}$ such that the dynamics converges to the stored state with maximal overlap with an initial (input) state. A proven choice of weights here can be found via the Hebbian learning rule

$$W_{ij} = \frac{1}{P} \sum_{p=1}^P w_p^i w_p^j. \quad (12)$$

Note that each associative memory of size N has a limited capacity, i.e. a maximal number of stored states, which can be reliably recalled. Convergence to a particular memory state is not guaranteed to succeed for an input state with too strong deviations or if too many states are stored.

In a quantum simulator one replaces Hopfield's classical spin update dynamics by quantum annealing to find the ground state of the Hamiltonian [34]

$$H_{AM} = -\sum_{i < j} W_{ij} \sigma_i^z \sigma_j^z - \nu \sum_i \chi_i \sigma_i^z, \quad (13)$$

where the first term corresponds to $E(\mathbf{s})$. The second term lowers the energy of states the more, the closer they are to the input state χ . For a proper choice of ν , the

ground state then corresponds to the memorized state with maximal overlap with χ . Note that in this implementation the input state is encoded in the local fields and not in the initial state as in the classical case.

Here H_{AM} (13) is given by the interaction matrix

$$A_{ij} = W_{ij} + \nu \chi_i \delta_{ij} \quad (14)$$

depending on memory and input states, such that the spin Hamiltonian (9) resembles the Hamiltonian in [34] except for the kinetic term. Physically each lattice site corresponds to a neuron with the two states ‘occupied’ and ‘not occupied’ and weights are determined by the pump lasers.

We now consider a specific example with 8 sites ($N = 8$) filled with 4 particles resulting in $\binom{8}{4} = 70$ possible states. We want to store two target states

$$\begin{aligned} \mathbf{w}_1 &= (1, 1, -1, -1, 1, -1, 1, -1) \\ \mathbf{w}_2 &= (1, 1, -1, 1, 1, -1, -1, -1). \end{aligned}$$

Choosing a third state as input state then fixes the interaction matrix (14) to implement. Annealing should then evolve to the memory state with bigger overlap.

Now we need to find $M = N(N + 1)/2 = 36$ suitable modes creating a basis of matrices $\mathcal{B} = \{V_m\}_{m=1,\dots,M}$. Here we assume a 1D lattice of depth $V_L = 10(\hbar k_L)^2/(2m_A)$ and spacing $d = 1.2\lambda_{n=100}/2$ in the z - r_L -plane of the cavity. It is illuminated from an orthogonal direction such that the pump fields are uniform along the lattice $u_{p,m}(x) = 1$. Thus the V_m ’s only depend on the cavity modes chosen from a candidate set of 300 Hermite-Gaussian modes with longitudinal mode index $n \in \{100, 199\}$ and transverse indices $l \in \{0, 1, 2\}$ and $m = 0$. For an appropriate cavity mirror radius to length ratio $R/L = 2/3$ their resonance frequencies are equidistant. Since we want to avoid nearly parallel coupling matrices V_m to keep the input parameters f_m as uniform as possible, we take the subset of M modes (defining \mathcal{B}) which maximizes the determinant of the Gram matrix of the normalized basis \mathcal{B}_{norm} (i.e. the volume spanned by the normalized V_m ’s).

Once the modes are chosen and \mathcal{B} is fixed we determine the input parameters $f_m(A)$ from eq. (10) rounded to one decimal place \tilde{f}_m . The recovered interaction matrix $\tilde{A}(\tilde{f}_1, \dots, \tilde{f}_M)$ (7) will then approximate A up to an accuracy depending on \mathcal{B} and \tilde{f}_m .

For the input pattern $\chi_1 = (1, 1, 1, -1, -1, -1, 1, -1)$ and $\nu = 0.7$ the eigenvalue spectrum of the Hamiltonian $H_{sp}(\zeta(t))$ is depicted in figure 2. As expected, for $\zeta \gg J$ the ground state converges to $|\mathbf{w}_1\rangle$ since the overlap $\chi_1 \cdot \mathbf{w}_1 = 4$ is larger than $\chi_1 \cdot \mathbf{w}_2 = 0$. We see that the minimum gap between ground and first excited state is $\Delta_{min} = 0.56J$ at $\zeta = 0.28J$. During an adiabatic sweep increasing ζ this is the most likely region for Landau-Zener tunneling from ground state to excited states. The typical behavior of the time-dependent solution of the

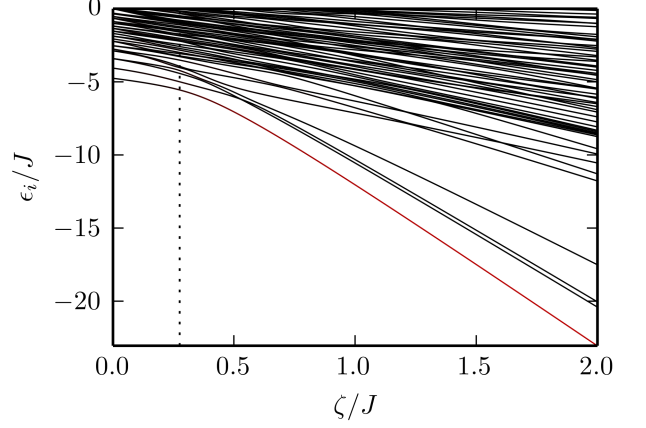


FIG. 2. Spectrum of the lowest few eigenvalues ϵ_i of H_{sp} (eq. (9)) as function of ζ . The recovered interaction matrix \tilde{A} used in H_{sp} also represents the input pattern $\chi_1 = (1, 1, -1, 1, 1, -1, -1, -1)$. The dotted line at $\zeta = 0.28J$ shows the position of the smallest gap between ground state and first excited state. The color of the lines shows the overlap of the target memory state $|\mathbf{w}_1\rangle$ with the eigenstates from black=0 to red=1.

Schrödinger equation for different annealing times τ is shown in figure 3 and indeed for slow enough scans the system converges to the desired target state.

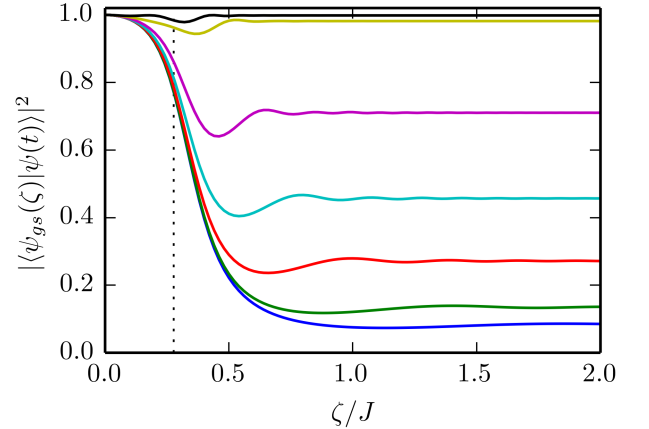


FIG. 3. Time evolution of overlap of the instantaneous ground state $|\psi_{gs}(\zeta)\rangle$ and the solution of the time-dependent Schrödinger equation $|\psi(t)\rangle$ for linear increase of ζ and different annealing times $J\tau = 1$ (blue), 2 (green), 5 (red), 10 (cyan), 20 (magenta), 50 (yellow) and 100 (black). The dotted line shows the smallest gap as above.

Conclusions.—Let us point out that the system studied here is not far from available experimental configurations as used at ETH [15] and Hamburg [8]. These need to be extended adding extra laser frequencies, as provided by current frequency comb technology. As cavity and comb

modes are equidistant, a single lock would be sufficient to bring many modes to resonance. While the general quadratic scaling of the number of lasers with the lattice sites number seems to be rather restrictive at first, the lasers are just a classical resource here. It also turns out that the required number of laser frequencies for a specific problem can be strongly reduced by applying the same laser from different angles.

In our example we found the desired state via adiabatic transfer. As said, for our open system, adiabatic transfer is not the only possibility as the ground state can also be reached via cavity side band cooling [33, 45] generalized to the multimode case.

Acknowledgements. We thank W. Lechner, T. Donner and J. Leonard for helpful discussions. This work is supported by the Austrian Science Fund Project I1697-N27.

-
- [1] H. Ritsch, P. Domokos, F. Brennecke, and T. Esslinger, *Reviews of Modern Physics* **85**, 553 (2013).
 - [2] A. T. Black, H. W. Chan, and V. Vuletić, *Physical Review Letters* **91**, 203001 (2003).
 - [3] S. Slama, G. Krenz, S. Bux, C. Zimmermann, and P. W. Courteille, *Physical Review A* **75**, 063620 (2007).
 - [4] P. Treutlein, D. Hunger, S. Camerer, T. W. Hänsch, and J. Reichel, *Physical Review Letters* **99**, 140403 (2007).
 - [5] S. Gupta, K. L. Moore, K. W. Murch, and D. M. Stamper-Kurn, *Physical review letters* **99**, 213601 (2007).
 - [6] K. Baumann, C. Guerlin, F. Brennecke, and T. Esslinger, *Nature* **464**, 1301 (2010).
 - [7] K. Arnold, M. Baden, and M. Barrett, *Physical review letters* **109**, 153002 (2012).
 - [8] H. Keßler, J. Klinder, M. Wolke, and A. Hemmerich, *Physical review letters* **113**, 070404 (2014).
 - [9] A. J. Kollár, A. T. Papageorge, K. Baumann, M. A. Armen, and B. L. Lev, *New Journal of Physics* **17**, 043012 (2015).
 - [10] P. Domokos and H. Ritsch, *Physical Review Letters* **89**, 253003 (2002).
 - [11] J. Keeling, M. Bhaseen, and B. Simons, *Physical review letters* **112**, 143002 (2014).
 - [12] F. Piazza and P. Strack, *Physical review letters* **112**, 143003 (2014).
 - [13] Y. Chen, Z. Yu, and H. Zhai, *Physical review letters* **112**, 143004 (2014).
 - [14] K. Hepp and E. H. Lieb, *Annals of Physics* **76**, 360 (1973).
 - [15] R. Landig, L. Hruby, N. Dogra, M. Landini, R. Mottl, T. Donner, and T. Esslinger, *Nature* (2016).
 - [16] Y. Li, L. He, and W. Hofstetter, *Physical Review A* **87**, 051604 (2013).
 - [17] M. R. Bakhtiari, A. Hemmerich, H. Ritsch, and M. Thorwart, *Physical review letters* **114**, 123601 (2015).
 - [18] S. Krämer and H. Ritsch, *Phys. Rev. A* **90**, 033833 (2014).
 - [19] V. Torggler and H. Ritsch, *Optica* **1**, 336 (2014).
 - [20] S. Gopalakrishnan, B. L. Lev, and P. M. Goldbart, *Nature Physics* **5**, 845 (2009).
 - [21] S. Gopalakrishnan, B. L. Lev, and P. M. Goldbart, *Physical review letters* **107**, 277201 (2011).
 - [22] S. Gopalakrishnan, B. L. Lev, and P. M. Goldbart, *Philosophical Magazine* **92**, 353 (2012).
 - [23] H. Habibian, A. Winter, S. Paganelli, H. Rieger, and G. Morigi, *Physical review letters* **110**, 075304 (2013).
 - [24] I. B. Mekhov and H. Ritsch, *Physical review letters* **102**, 020403 (2009).
 - [25] S. F. Caballero-Benitez and I. B. Mekhov, *Physical review letters* **115**, 243604 (2015).
 - [26] A. J. Kollár, A. T. Papageorge, V. D. Vaidya, Y. Guo, J. Keeling, and B. L. Lev, *arXiv preprint arXiv:1606.04127* (2016).
 - [27] P. Hauke, L. Bonnes, M. Heyl, and W. Lechner, *Frontiers in Physics* **3**, 21 (2015).
 - [28] M. Johnson, M. Amin, S. Gildert, T. Lanting, F. Hamze, N. Dickson, R. Harris, A. Berkley, J. Johansson, P. Bunyk, *et al.*, *Nature* **473**, 194 (2011).
 - [29] V. Choi, *Quantum Information Processing* **7**, 193 (2008).
 - [30] W. Lechner, P. Hauke, and P. Zoller, *Science advances* **1**, e1500838 (2015).
 - [31] T. Kadowaki and H. Nishimori, *Physical Review E* **58**, 5355 (1998).
 - [32] E. Farhi, J. Goldstone, S. Gutmann, J. Lapan, A. Lundgren, and D. Preda, *Science* **292**, 472 (2001).
 - [33] R. M. Sandner, W. Niedenzu, F. Piazza, and H. Ritsch, *EPL (Europhysics Letters)* **111**, 53001 (2015).
 - [34] S. Santra, O. Shehab, and R. Balu, *arXiv preprint arXiv:1602.08149* (2016).
 - [35] C. Maschler, I. B. Mekhov, and H. Ritsch, *The European Physical Journal D* **46**, 545 (2008).
 - [36] C. Maschler and H. Ritsch, *Physical review letters* **95**, 260401 (2005).
 - [37] I. B. Mekhov and H. Ritsch, *Journal of Physics B: Atomic, Molecular and Optical Physics* **45**, 102001 (2012).
 - [38] D. Jaksch, C. Bruder, J. I. Cirac, C. W. Gardiner, and P. Zoller, *Physical Review Letters* **81**, 3108 (1998).
 - [39] D. Sherrington and S. Kirkpatrick, *Physical review letters* **35**, 1792 (1975).
 - [40] G. E. Santoro and E. Tosatti, *Journal of Physics A: Mathematical and General* **39**, R393 (2006).
 - [41] S. Boixo, T. F. Rønnow, S. V. Isakov, Z. Wang, D. Wecker, D. A. Lidar, J. M. Martinis, and M. Troyer, *Nature Physics* **10**, 218 (2014).
 - [42] B. Heim, T. F. Rønnow, S. V. Isakov, and M. Troyer, *Science* **348**, 215 (2015).
 - [43] H. G. Katzgraber, F. Hamze, Z. Zhu, A. J. Ochoa, and H. Muñoz-Bauza, *Physical Review X* **5**, 031026 (2015).
 - [44] T. Kato, *Journal of the Physical Society of Japan* **5**, 435 (1950).
 - [45] M. Wolke, J. Klinner, H. Keßler, and A. Hemmerich, *Science* **337**, 75 (2012).
 - [46] J. J. Hopfield, *Proceedings of the national academy of sciences* **79**, 2554 (1982).